



Cite this: *Phys. Chem. Chem. Phys.*,
2016, **18**, 15727

Cluster size and composition dependent water deprotonation by free manganese oxide clusters†

Sandra M. Lang,^{*ae} Thorsten M. Bernhardt,^a Denis M. Kiawi,^{bc} Joost M. Bakker,^{*b}
Robert N. Barnett^d and Uzi Landman^{*d}

In the quest for cheap and earth abundant but highly effective and energy efficient water splitting catalysts, manganese oxide represents one of the materials of choice. In the framework of a new hierarchical modeling strategy we employ free non-ligated manganese oxide clusters $Mn_xO_{x+y}^+$ ($x = 2-5$, $y = -1, 0, 1, 2$) as simplified molecular models to probe the interaction of water with nano-scale manganese oxide materials. Infrared multiple-photon dissociation (IR-MPD) spectroscopy in conjunction with first-principles spin density functional theory calculations is applied to study several series of $Mn_xO_{x+y}(H_2O)_n^+$ complexes and reveal that the reaction of water with $Mn_xO_{x+y}^+$ leads to the deprotonation of the water molecules via hydroxylation of the cluster oxo-bridges. This process is independent of the formal Mn oxidation state and occurs already for the first adsorbed water molecule and it proceeds until all oxo-bridges are hydroxylated. Additional water molecules are bound intact and favorably form H_3O_2 units with the hydroxylated oxo-bridges. Water adsorption and deprotonation is also found to induce structural transformations of the cluster core, including dimensionality crossover. Furthermore, the IR-MPD measurements reveal that clusters with one oxygen atom in excess $Mn_xO_{x+1}^+$ contain a terminal O atom while clusters with two oxygen atoms in excess $Mn_xO_{x+2}^+$ contain an intact O_2 molecule which, however, dissociates upon adsorption of a minimum number of water molecules. These basic concepts could aid the future design of artificial water-splitting molecular catalysts.

Received 3rd February 2016,
Accepted 20th May 2016

DOI: 10.1039/c6cp00779a

www.rsc.org/pccp

1. Introduction

The development of cheap, earth abundant, and non-toxic materials which serve as effective and energy efficient catalysts for the artificial splitting and oxidation of water represents one of the biggest challenges in current catalysis research. In nature this reaction is catalyzed within photosystem II (PS II). Recent X-ray diffraction studies^{1,2} revealed that the catalytically active center consists of an inorganic $CaMn_4O_5$ cluster which, together with its protein ligands, forms the oxygen evolving complex (OEC) of PS II.

Besides these structural investigations great efforts have also been invested in the elucidation of the catalytic water oxidation mechanism. While considerable progress has been made in this direction leading to the proposal of several reaction schemes,²⁻⁴ the interaction of water molecules with the OEC and the subsequent oxidation of water is still not completely understood on a molecular level.

The naturally occurring and thus highly abundant and optimized catalyst has inspired the preparation of numerous functional synthetic analogues of the OEC containing bi- and tetra-nuclear manganese oxide complexes.^{5,6} Furthermore, solid manganese oxide and calcium-manganese oxide materials have been used as biomimetic water splitting catalysts.^{6,7} However, to probe basic concepts which could further aid the design of artificial water splitting catalysts, the development of novel model systems which provide a fundamental and conceptual understanding of the interaction of water with the $CaMn_4O_5$ cluster is mandatory.

Toward this goal we have recently embarked on a novel hierarchical modeling strategy by starting from an elementary model and increasing the complexity of the model system in a staged, controlled manner. In a first step we have employed a free non-ligated cluster $Mn_4O_4^+$ comprised of the earth abundant and non-toxic elements manganese and oxygen.

^a Institute of Surface Chemistry and Catalysis, University of Ulm,
Albert-Einstein-Allee 47, 89069 Ulm, Germany. E-mail: sandra.lang@uni-ulm.de

^b Radboud University, Institute for Molecules and Materials, FELIX Laboratory,
Toernooiveld 7, 6525 ED Nijmegen, The Netherlands.
E-mail: j.bakker@science.ru.nl

^c Anton Pannekoek Institute, University of Amsterdam, Science Park 904,
1098 XH Amsterdam, The Netherlands

^d School of Physics, Georgia Institute of Technology, Atlanta, Georgia 30332-0430,
USA. E-mail: uzi.landman@physics.gatech.edu

^e Institute of Chemical Engineering, University of Ulm, Albert-Einstein-Allee 11,
89081 Ulm, Germany

† Electronic supplementary information (ESI) available: Theoretical method and detailed information about spin density and charge distributions as well as the bonding of terminal oxygen. See DOI: 10.1039/c6cp00779a

Recent reactivity studies of this Mn_4O_4^+ cluster with D_2^{16}O and H_2^{18}O in a gas phase ion trap apparatus revealed the fast adsorption of multiple water molecules as well as the facile exchange of the oxygen atom of the cluster with water oxygen atoms.^{8,9} This provided for the first time direct experimental evidence for the ability of Mn_4O_4^+ to deprotonate water *via* hydroxylation of the cluster oxo-bridges. Concurrent first-principles spin-density-functional theory (SDFT) simulations provided new fundamental insight into the mechanism and energetics of the water binding and deprotonation process. In particular, a water-induced dimensionality change from a two-dimensional ring-like ground state structure of the bare Mn_4O_4^+ (in contrast to previous calculations,¹⁰ a similar ring-like structure has recently also been found for neutral^{8,11} Mn_4O_4) to a cuboidal tetra-water adsorption complex $\text{Mn}_4\text{O}_4(\text{H}_2\text{O})_4^+$ has been predicted. The resulting three-dimensional cuboid has been found to comprise a structure with μ_3 -bridging oxygen atoms similar to the structure of the inorganic core of the OEC. Furthermore, it has been shown that this dimensionality change facilitates the subsequent splitting of the water molecules of $\text{Mn}_4\text{O}_4(\text{H}_2\text{O})_4^+$ to yield the octa-hydroxy complex $(\text{MnOH})_4(\text{OH})_4^+$.

For a more detailed insight into the interaction of water with Mn_4O_4^+ and into the cluster's ability to deprotonate water we have recently presented a systematic investigation of a series of $\text{Mn}_4\text{O}_4(\text{H}_2\text{O})_n^+$ ($n = 1-7$) complexes in which we employed first-principles SDFT calculations in conjunction with infrared multiple-photon dissociation (IR-MPD) spectroscopy.¹² This study revealed that the splitting of the O-H bond of water through hydroxylation of Mn-O-Mn μ -oxo bridges is central to the interaction of water molecules with Mn_4O_4^+ . This reaction has been found to occur already for the first adsorbed H_2O molecule and continues for all subsequent water adsorption reactions until all available μ -oxo-bridges are hydroxylated. Further water molecules are observed to bind molecularly with a preference for the formation of hydrogen-bridge-bound H_3O_2 units. Furthermore, the Mn_4O_4^+ cluster unit appeared to be highly structurally fluxional and the adsorbed water ligands induce structural transformations of the cluster core. Starting from a two-dimensional (2D) ring-like structure of bare Mn_4O_4^+ it transforms into a 2D square-like ground-state (or a 2D ladder-like isomer) arrangement of $\text{Mn}_4\text{O}_4(\text{H}_2\text{O})^+$, and culminates with an increasing number of water molecules ($n \geq 2$) with three-dimensional (3D) cuboidal geometries. First for $\text{Mn}_4\text{O}_4(\text{H}_2\text{O})_n^+$ ($n \leq 5$) open cuboids have been found while closed ones emerge for an increasing number of adsorbed water molecules, *i.e.* $\text{Mn}_4\text{O}_4(\text{H}_2\text{O})_n^+$ ($n \geq 6$).

In order to probe the generality of these findings and to formulate universal concepts for the interaction of water with manganese oxide clusters we have now extended the previous investigations to a series of $\text{Mn}_x\text{O}_x(\text{H}_2\text{O})_n^+$ complexes in the size range between two and five manganese atoms. To elucidate a potential influence of the Mn formal oxidation state on the water deprotonation, also oxygen-rich clusters $\text{Mn}_x\text{O}_{x+1}(\text{H}_2\text{O})_n^+$ ($x = 2-4$) and $\text{Mn}_x\text{O}_{x+2}(\text{H}_2\text{O})_n^+$ ($x = 2-4$) as well as the oxygen-deficient $\text{Mn}_4\text{O}_3(\text{H}_2\text{O})_n^+$ complexes have been included. This issue is particularly interesting since the subsequent oxidation of water to molecular oxygen has been found to be strongly

dependent on the Mn oxidation state.^{4,13} The experimental IR-MPD findings for $\text{Mn}_2\text{O}_2(\text{H}_2\text{O})_n^+$ and $\text{Mn}_4\text{O}_4(\text{H}_2\text{O})_n^+$ pertaining to the vibrational characteristics of the clusters are analyzed with the use of concurrent first-principles SDFT calculations, through which we gain comprehensive understanding about the size-dependent evolution of the clusters' structural motifs and insight into the fluxionality of the cluster cores.

2. Methods

2.1 Experimental methods

Cationic manganese oxide clusters are produced by pulsed laser ablation of a manganese sample rod (Goodfellow, purity 99.99%) using the second harmonic of a Nd:YAG laser (532 nm, Brio Quantel, attenuated to approximately 30 mJ per pulse). The sample is rotated and translated by a stepper motor enabling a homogeneous erosion of the rod. Ablation takes place in a 4 mm diameter flow tube type cluster growth channel in the presence of a helium carrier gas seeded with 0.5% oxygen that is introduced through a pulsed valve. To form cluster-water complexes, a mixture of 1% water vapor in helium is introduced 60 mm downstream of the sample rod.

On exiting the flow reactor the reaction mixture is expanded into vacuum forming a molecular beam that travels toward the extraction region of a reflectron time-of-flight mass spectrometer. Here, the clusters interact with the IR laser beam (produced by the Free Electron Laser for Infrared eXperiments, FELIX, 300–1700 cm^{-1} , 10 μs pulse duration).¹⁴ The light has a spectral bandwidth that is kept to 0.3% RMS (root mean square) of the central frequency. A few μs after interaction with FELIX, all clusters are pulse-extracted into the mass spectrometer and detected with a microchannel plate detector. To correct for long term source fluctuations, the experiment is operated at twice the FELIX repetition rate, allowing for the recording of reference mass spectra in between successive FELIX pulses.

Whenever FELIX is in resonance with a vibrational mode of a given cluster, the number of $\text{Mn}_x\text{O}_{x+y}(\text{H}_2\text{O})_n^+$ cations detected is depleted due to dissociation of the complex. This means that the ratio of the mass peak intensity obtained with (I) and without (I_0) laser light, I/I_0 , becomes smaller than one ($I/I_0 < 1$). The fragmentation leads to a signal gain of the fragmentation product ($I/I_0 > 1$). Since no mass-selection has been performed prior to the interaction with the laser, the IR-MPD spectrum of one specific cluster complex can also exhibit overlapping features of depletion and gain. To minimize the extent of the overlap between depletion and gain, the IR-MPD spectra shown below have been obtained in different experimental runs under different experimental conditions. In particular, the number of adsorbed water molecules has been controlled by changing the amount of water introduced in the flow tube reactor.

2.2 Theoretical methods

The theoretical explorations of the atomic arrangements and electronic structures of the bare manganese oxide clusters and their water complexes were performed with the use of the

Born–Oppenheimer spin-density-functional theory molecular dynamics (BO-SDFT-MD) method¹⁵ with norm-conserving soft (scalar relativistic for Mn) pseudopotentials¹⁶ and the generalized gradient approximation (GGA)¹⁷ for electronic exchange and correlations. The BO-SDFT-MD method¹⁵ is particularly suitable for investigations of charged systems since it does not employ a supercell (*i.e.*, no periodic replication of the ionic system is used); for further details see the ESI.†

In all the calculations the dependence on spin multiplicity has been checked, and the results that we report correspond to the spin multiplicities with the lowest energies (global minimum for the ground-state configuration, and local minimum for the isomeric structures); both spin and geometrical isomers are explored. The cluster is initially set up using atomic wave functions, with each iron atom having either five up-spin, or five down-spin, 3d orbitals fully occupied. All possible combinations are tried, including geometry optimization with the orbital occupancy determined by the Fermi distribution function. Evaluation of the energy of the cationic clusters started with removal of an electron from the highest occupied orbital followed by optimization of the cluster geometry and occupancy. We have also tested some cases in which the Fe atoms were not initialized with fully occupied majority spin 3d orbitals, but these failed to yield a lower final energy. In the following we denote the difference between the spin-up and spin-down electrons by $\mu = N_{\uparrow} - N_{\downarrow}$. For analysis of the spatial distribution of the majority and minority spin density-distributions and antiferromagnetic cluster configurations see our discussion below in connection with Fig. 4 and 6 and the ESI.†

The energy minimization to find the optimal cluster geometry was done with a steepest-descent method. The convergence criteria were that the maximum force magnitude on any particle is less than 0.0005 Hartree per Bohr (Hartree = 2 Ry \approx 27.211 eV, Bohr = $a_0 \approx$ 0.529 Å) and that the average over all particles is less than 0.00025 Hartree per Bohr.

The eigenmode frequencies and eigenvectors are determined in the harmonic approximation by direct diagonalization of the dynamical matrix, constructed by finite differencing of the forces at different points near the equilibrium geometry.¹⁸ From the DFT calculations for the displacements we also evaluate for each of the atoms the effective-charge tensor (the derivative of the dipole of the system with respect to the displacement of the atom), which together with the eigenmode vectors yields the oscillator strengths of the vibrational modes and the IR intensities.¹⁹ In addition we calculate for each normal mode frequency ν_j the density of states (DOS) projected on each of the atoms;¹² (more details are given in the ESI.†); see projected vibrational DOS, pvDOS in Fig. 1.

3. Results and discussion

3.1 Assignment of vibrational modes

To assign characteristic vibrational modes of the water complexes $\text{Mn}_x\text{O}_{x+y}(\text{H}_2\text{O})_n^+$ and to understand the experimentally obtained IR-MPD spectra, it is imperative that the energy-optimal structures of the clusters' ground states and their higher-energy

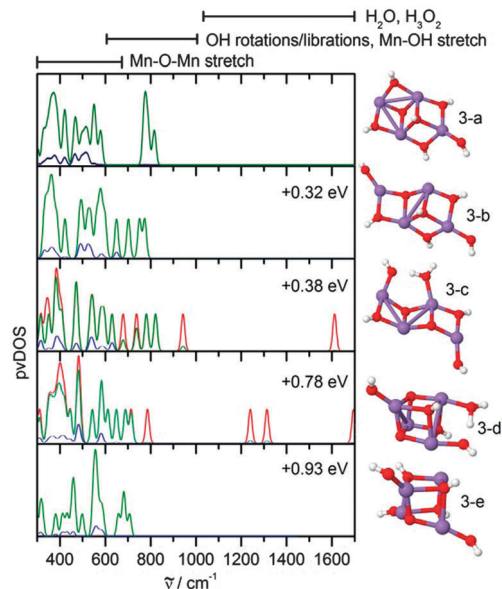


Fig. 1 Projected vibrational density of states (pvDOS, per cm^{-1}) for five different isomeric structures of $\text{Mn}_4\text{O}_4(\text{H}_2\text{O})_3^+$. The red curves represent the total vDOS whereas the green curve characterizes vibrational displacements of Mn atoms, the O atoms, and OH groups. The blue curve is the projection on the Mn atoms. For isomers 3-a (the ground state) and 3-b the red and green curves overlap in the whole frequency range obscuring the red curve. The presented curves are obtained by convolution of the discrete values of the vDOS with a Gaussian line shape function with a FWHM of 8 cm^{-1} . In the structural models, Mn, O, and H atoms are depicted as purple, red, and white spheres, respectively.

isomers be determined and that their vibrational properties be calculated and analyzed. As the congestion of normal modes for these systems precludes a facile individual characterization, we have calculated for each normal mode frequency the DOS projected on each of the atoms. By combining the projections on certain atoms or side groups one can identify their vibrational contributions to the complete vibrational spectrum. As an example Fig. 1 displays the total vibrational density of states, vDOS (red curves), as well as the projected vibrational density of states (pvDOS, green and blue curves) for the ground state and four higher energy isomeric structures of the complex $\text{Mn}_4\text{O}_4(\text{H}_2\text{O})_3^+$.

Isomer 3-a, corresponding to the minimum energy (ground state) isomer, as well as isomers 3-b (+0.32 eV higher in energy relative to the ground state) and 3-e (+0.93 eV above the ground state) contain deprotonated water whereas isomers 3-c (+0.38 eV) and 3-d (+0.78 eV) contain one intact water molecule each. Isomer 3-a consists of two joined (sharing a face) open cuboids (both missing a corner). Five of the cluster oxo-bridges are hydroxylated resulting from the dissociation of all three adsorbed water molecules. Isomer 3-b exhibits an open cuboidal Mn_3O_4 unit to which the fourth Mn atom is coordinated *via* one of the corner oxygen atoms. Three of the cluster oxo-bridges are hydroxylated resulting from the dissociation of all three adsorbed water molecules. A similar, however, more open structure is also found for isomer 3-c. In contrast, isomers 3-d and 3-e have a cuboidal Mn_4O_4 cluster core.

The blue curves in Fig. 1 characterize vibrational displacements of the Mn atoms, the green curves characterize vibrational displacements of the Mn atoms, the O atoms, and OH groups, and the red curves characterize the total vibrational displacements of all Mn and O atoms as well as OH, H₂O and H₃O₂ units. Consequently, the difference between the red and green curves represents the contributions of H₂O and H₃O₂ units to the vibrational density of states, the difference between the green and blue curve represents the contributions of O atoms and OH groups, and the blue curve corresponds to the contributions of the Mn atoms. This also means, whenever the red curve is not visible (like for example for 3-a and 3-b) there are no contributions from H₂O or H₃O₂ units and the total vDOS is described by the green curve, *i.e.* the red and green curves completely overlap.

This pvDOS analysis allows for the assignment of three distinct regions: (1) for all five isomers the region below 600 cm⁻¹ is dominated by the blue and green curve and thus these vibrations correspond to Mn–O–Mn motions of the cluster core. (2) The region between about 600 cm⁻¹ and 1000 cm⁻¹ is dominated by the green curve and the vibrations can be mainly assigned to modes associated with vibrational displacements of OH subunits, in particular librations and rotations of the OH groups and Mn–OH stretch vibrations. In addition, the spectra of isomers 3-c and 3-d show that the red and green curves do not completely overlap in this region. These features arise from librations of intact water molecules. (3) At wavenumbers larger than 1000 cm⁻¹ no modes are observed for isomer 3-a, 3-b and 3-e whereas the spectra of the isomers 3-c and 3-d are dominated by the red curve. This means, that these vibrations typically arise from vibrational displacements of H₂O and H₃O₂ groups. The most characteristic mode in this spectral region is the HOH bending motion, which is typically found between 1500 cm⁻¹ and 1700 cm⁻¹. Isomers 3-a, 3-b and 3-e contain only deprotonated water and thus do not have any modes in this region. In contrast, isomers 3-c and 3-d bind one intact water molecule which is reflected by the appearance of an HOH bending mode at 1615.5 cm⁻¹ (3-c) and 1698.7 cm⁻¹ (3-d), respectively. Higher energy vibrations corresponding to the symmetric and asymmetric OH vibrational modes appear at wavenumbers larger than 3500 cm⁻¹ and are not shown in Fig. 1.

This assignment of the vibrational modes to characteristic wavenumber regions is found to be valid for all investigated Mn_xO_{x+y}(H₂O)_n⁺ complexes.

3.2 Size and composition dependent water deprotonation

The most characteristic vibrational mode to explore the ability of the Mn_xO_{x+y}⁺ clusters to deprotonate water is the HOH bending mode. For a free H₂O molecule²⁰ this mode has a wavenumber of 1595 cm⁻¹ while it can typically be found at wavenumbers in the range of 1500–1700 cm⁻¹ for intact water molecules adsorbed on a Mn_xO_{x+y}⁺ cluster (*cf.* Section 3.1 and Fig. 1). In marked contrast, the water bending mode disappears upon dissociation (deprotonation) of the water molecules.¹²

Fig. 2 displays, as an example, the IR-MPD spectra recorded on the mass signals corresponding to the di-manganese di-oxygen

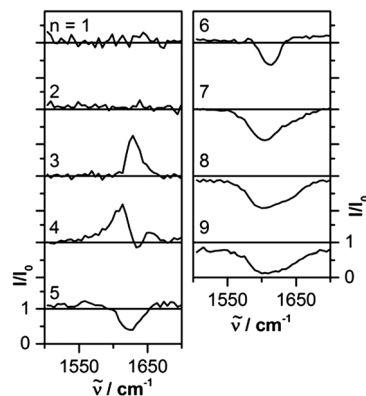


Fig. 2 Measured IR-MPD spectra of the complexes Mn₂O₂(H₂O)_n⁺ (*n* = 1–9) in the spectral region of 1500–1700 cm⁻¹ which is characteristic for the HOH bending mode of intact water molecules. Plotted is the mass signal intensity ratio *I*/*I*₀ with (*I*) and without (*I*₀) laser light, as a function of the incident laser wavenumber $\tilde{\nu}$.

water complexes Mn₂O₂(H₂O)_n⁺ (*n* = 1–9) in the characteristic HOH bending mode region of 1500–1700 cm⁻¹. These spectra show the ratio of the mass peak intensity obtained with (*I*) and without (*I*₀) laser light. When the light is not resonant with a vibrational transition, no fragmentation occurs and the ratio *I*/*I*₀ is 1. In case of resonant absorption of IR light the cluster complex fragments and the ratio *I*/*I*₀ becomes smaller than 1 which appears as a “depletion” in the IR-MPD spectrum. At the same time this fragmentation causes an intensity “gain” on the mass signal of the corresponding fragmentation product which is reflected by a *I*/*I*₀ value larger than 1.

The first three spectra recorded on the masses of Mn₂O₂(H₂O)_{1–3}⁺ do not exhibit any depletion signal (*I*/*I*₀ < 1) in the shown spectral region. This indicates that the first three water molecules are not bound intact but are deprotonated on Mn₂O₂⁺. In contrast, the spectrum of Mn₂O₂(H₂O)₄⁺ has a double peak structure which we interpret to be caused by an overlap of a depletion signal and a gain signal. On the one hand, Mn₂O₂(H₂O)₄⁺ absorbs light and fragments at a center wavenumber of 1630 cm⁻¹ (with full width at half maximum (FWHM) of 23 cm⁻¹) *via* loss of one water molecule



to form the depletion signal. This fragmentation process is reflected by a simultaneous gain signal in the Mn₂O₂(H₂O)₃⁺ mass channel. The gain signal in Mn₂O₂(H₂O)₄⁺ is due to fragmentation of Mn₂O₂(H₂O)₅⁺



which absorbs at a center wavenumber of 1624 cm⁻¹ (FWHM 35 cm⁻¹). All larger complexes Mn₂O₂(H₂O)_{6–9}⁺ exhibit a clear depletion feature at center wavenumbers of 1612 cm⁻¹, 1608 cm⁻¹, 1612 cm⁻¹, and 1614 cm⁻¹, respectively, indicating that these complexes contain at least one intact water molecule. Thus, Mn₂O₂(H₂O)₄⁺ represents the smallest complex which exhibits a depletion corresponding to an HOH bending mode. Furthermore, the spectra show that the peak width (FWHM) broadens

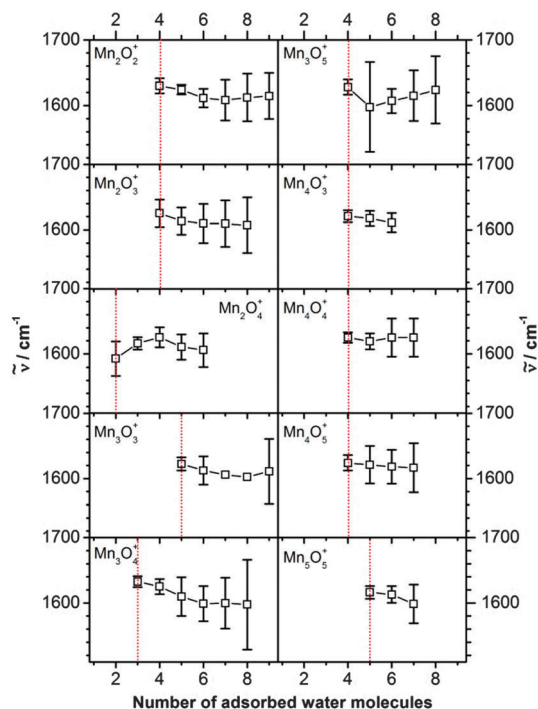


Fig. 3 Experimentally obtained band centers for the HOH bending mode as a function of the adsorbed water molecules on $\text{Mn}_2\text{O}_{2+y}^+$ ($y = 0-2$), $\text{Mn}_3\text{O}_{2+y}^+$ ($y = 0-2$), $\text{Mn}_4\text{O}_{2+y}^+$ ($y = -1, 0, 1$), and Mn_5O_5^+ . The error bars represent the signal width obtained at full width at half maximum (FWHM). The red dotted lines indicate the smallest complexes which show a depletion signal in the HOH bending mode region and thus contain at least one intact water molecule. The black lines are drawn to guide the eye.

with increasing water content from values smaller than 40 cm^{-1} for $\text{Mn}_2\text{O}_2(\text{H}_2\text{O})_{4-6}^+$ to about 70 cm^{-1} for $\text{Mn}_2\text{O}_2(\text{H}_2\text{O})_{8,9}^+$.

IR-MPD spectra as shown for the example of $\text{Mn}_2\text{O}_2(\text{H}_2\text{O})_n^+$ have been obtained for different series of di-, tri-, tetra-, and penta-manganese oxide water complexes. The obtained band centers of the HOH bending mode as a function of the number of adsorbed water molecules are shown in Fig. 3. The error bars mirror the corresponding peak width, *i.e.* the FWHM value. Generally, a broadening of the signals is observed with an increasing number of adsorbed water molecules. This could indicate the presence of different isomeric structures and/or the presence of multiple slightly differently bound water molecules.

Fig. 3 illustrates that the smallest complexes which show a depletion signal in the HOH bending mode region and thus contain at least one intact water molecule are $\text{Mn}_2\text{O}_2(\text{H}_2\text{O})_4^+$, $\text{Mn}_2\text{O}_3(\text{H}_2\text{O})_4^+$, $\text{Mn}_2\text{O}_4(\text{H}_2\text{O})_2^+$, $\text{Mn}_3\text{O}_3(\text{H}_2\text{O})_5^+$, $\text{Mn}_3\text{O}_4(\text{H}_2\text{O})_3^+$, $\text{Mn}_3\text{O}_5(\text{H}_2\text{O})_4^+$, $\text{Mn}_4\text{O}_3(\text{H}_2\text{O})_4^+$, $\text{Mn}_4\text{O}_4(\text{H}_2\text{O})_4^+$, $\text{Mn}_4\text{O}_5(\text{H}_2\text{O})_4^+$, and $\text{Mn}_5\text{O}_5(\text{H}_2\text{O})_5^+$.

In case of Mn_2O_3^+ and Mn_4O_3^+ , the smallest complexes, which exhibit a depletion signal corresponding to the HOH bending mode, contain four water molecules. This demonstrates that the first three water molecules deprotonate upon adsorption, *i.e.* the maximum number of dissociatively bound H_2O molecules n_{max} is equal to the number of oxygen atoms $x + y$ in the cluster core, $n_{\text{max}} = x + y$.

In contrast, for Mn_2O_4^+ , Mn_3O_4^+ , Mn_3O_5^+ , Mn_4O_4^+ , Mn_4O_5^+ , and Mn_5O_5^+ a depletion signal is observed for complexes

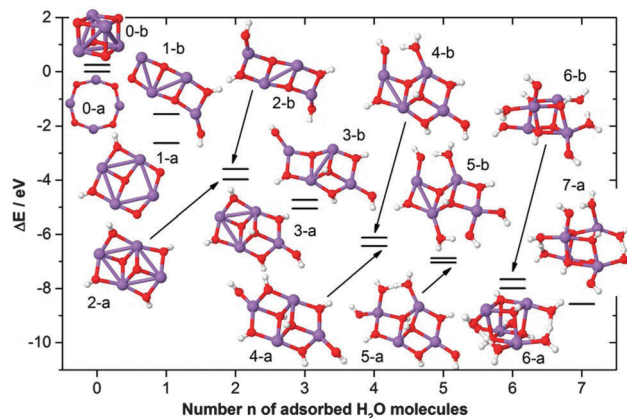


Fig. 4 Calculated binding energies of n water molecules to Mn_4O_4^+ for the two lowest (except for $\text{Mn}_4\text{O}_4(\text{H}_2\text{O})_7^+$) energy isomers (denoted as energy difference ΔE with respect to the bare ring-like Mn_4O_4^+ cluster), plotted along with the corresponding structures.¹² Mn, O, and H atoms are depicted as purple, red, and white spheres, respectively.

containing less or the same number of water molecules as oxygen atoms, *i.e.* the maximum number of dissociatively bound H_2O molecules is smaller than the number of oxygen atoms in the cluster, $n_{\text{max}} < x + y$.

To gain further insight into this phenomenon we have theoretically investigated the geometric structure of the series of $\text{Mn}_4\text{O}_4(\text{H}_2\text{O})_n^+$ complexes.¹² Fig. 4 displays the calculated binding energies (horizontal lines) of up to seven water molecules to Mn_4O_4^+ . Shown are the binding energies as well as the corresponding geometric structures for the two lowest energy (geometric) isomers. For all cases discussed in this paper, the lowest energy isomers of the ionized clusters are found to have a high-spin configuration (maximal number of majority spin electrons) regardless of the number of adsorbed water molecules; that is, for $\text{Mn}_4\text{O}_4(\text{H}_2\text{O})_n^+$ $\mu = 19$; in general for $\text{Mn}_x\text{O}_x(\text{H}_2\text{O})_n^+$ ($x = 2, 3, 4$ and $n = 0, 1, 2, \dots$), the highest $\mu = 5x - 1$. Spin isomers corresponding to the geometric isomers, 0-a, 0-b and 4-a in Fig. 4 are discussed in the ESI,[†] where spatial spin distributions (ferromagnetic for the maximal μ , and antiferromagnetic for smaller values of μ) and their localization on the manganese sites, are shown.

Regardless of the number of adsorbed water molecules, all minimum energy structures (labeled 1-a to 7-a) contain deprotonated water. The smallest complexes $\text{Mn}_4\text{O}_4(\text{H}_2\text{O})_{1-4}^+$ contain only deprotonated water while the larger complexes $\text{Mn}_4\text{O}_4(\text{H}_2\text{O})_{5-7}^+$ contain four dissociatively and $(n - 4)$ molecularly adsorbed H_2O molecules. The latter preferably form hydrogen bonded H_3O_2 subunits with neighboring hydroxyl groups as will be further discussed in Section 3.3. In contrast, higher energy isomers (with the exception of 1-b, 2-b and 3-b) bind at least one intact water molecule.

The IR-MPD spectra¹² show that already $\text{Mn}_4\text{O}_4(\text{H}_2\text{O})_4^+$ exhibits a depletion signal at a center wavenumber of 1624 cm^{-1} . This observed bending mode is consistent with the first higher energy isomer (4-b) which comprises one non-dissociated molecularly bound water molecule with a calculated HOH bending mode

at 1621 cm^{-1} . In the present experimental approach, the water complexes are formed under high pressure conditions and subsequently quenched in a supersonic expansion. This makes the stabilization and thus the presence of higher energy isomers likely as has also been shown previously for other systems.²¹ However, the coexistence of isomer 4-a which does not have the characteristic HOH bending mode cannot be ruled out.¹²

The calculations demonstrate that water deprotonation on Mn_4O_4^+ is preferred to occur *via* a 1,3-hydrogen shift resulting in the hydroxylation of the Mn–O–Mn μ -oxo bridges.^{8,12} This limits the number of water molecules which can dissociate on the cluster to the number of available cluster oxo-bridges. The observation of a maximum of three deprotonated water molecules on Mn_2O_3^+ and Mn_4O_3^+ , and thus, $n_{\text{max}} = x + y$, is in agreement with this theoretical prediction. For Mn_4O_4^+ the observation of a complex with only three deprotonated water molecules can be explained by the (co-)existence of the higher energy isomer 4-b. However, the calculations clearly show that a fourth water molecule can dissociate on the cluster and that also in this case, the maximum number n_{max} of dissociatively bound water molecules is determined by the number of cluster oxygen atoms. Similarly, the complexes $\text{Mn}_2\text{O}_4(\text{H}_2\text{O})_2^+$, $\text{Mn}_3\text{O}_4(\text{H}_2\text{O})_3^+$, $\text{Mn}_3\text{O}_5(\text{H}_2\text{O})_4^+$, $\text{Mn}_4\text{O}_5(\text{H}_2\text{O})_4^+$, and $\text{Mn}_5\text{O}_5(\text{H}_2\text{O})_5^+$ contain at least one intact water molecule although there are still cluster oxygen atoms available for hydroxylation. This similarity to Mn_4O_4^+ indicates a similar water deprotonation mechanism on these clusters and the potential stabilization of higher energy isomers.

Furthermore, from examination of the ground states in Fig. 4 we observe that (in the ground state) the Mn_4O_4^+ cluster core undergoes a structural evolution upon adsorption of multiple water molecules. The bare cluster (0-a) has a 2D ring-like geometry which transforms to a 2D mixed ring-ladder-like structure after dissociative adsorption of the first water molecule (1-a). A 3D structure emerges upon the adsorption of two water molecules (2-a), and it further develops upon the adsorption of a third water molecule into a 3D cluster core comprising a Mn_3O_4 unit which forms an open cube (with one vertex missing) and the fourth Mn atom coordinated to the open cube *via* one of the corner oxygen atoms and an additional oxygen atom (3-a). This structural motif is retained for the adsorption of a total of five water molecules. Upon adsorption of a sixth H_2O a final structural change to a cuboidal geometry (6-a) is observed which represents the minimum energy geometry for all larger water complexes. This behavior shows that the Mn_4O_4^+ cluster is structurally highly fluxional. This is in agreement with previous reactivity studies using isotopic water, H_2^{18}O , which demonstrated facile exchange of cluster oxygen atoms with oxygen atoms of the water molecules, in a process that requires opening of the cluster structure and thus a high structural fluxionality.⁹

So far, we have found that for all the discussed clusters deprotonation of water favorably occurs *via* hydroxylation of the cluster oxygen atoms and accordingly, the observed number of deprotonated water molecules is smaller or equal to the number of available cluster O atoms. In marked contrast, for Mn_2O_2^+ and Mn_3O_3^+ the smallest complexes which exhibit a depletion signal

corresponding to the HOH bending mode are $\text{Mn}_2\text{O}_2(\text{H}_2\text{O})_4^+$ and $\text{Mn}_3\text{O}_3(\text{H}_2\text{O})_5^+$. This indicates that up to three and four water molecules, respectively, bind dissociatively to these clusters. Since this number is larger than the number of available cluster oxygen atoms this observation suggests a different mechanism for water deprotonation or a new structural motif which can explain the absence of the HOH bending mode for the smaller complexes $\text{Mn}_2\text{O}_2(\text{H}_2\text{O})_3^+$ and $\text{Mn}_3\text{O}_3(\text{H}_2\text{O})_4^+$.

3.3 Formation of H_3O_2 units

To understand the lack of the HOH bending mode for these clusters first-principles simulations have been performed for the series of $\text{Mn}_2\text{O}_2(\text{H}_2\text{O})_n^+$ ($n = 0-8$) complexes. As an example, Fig. 5 displays the experimental IR-MPD spectrum of $\text{Mn}_2\text{O}_2(\text{H}_2\text{O})_3^+$ in the whole investigated wavenumber range of $300-1700\text{ cm}^{-1}$ together with calculated spectra for the two lowest energy isomers. This complex has been chosen since it represents the largest $\text{Mn}_2\text{O}_2(\text{H}_2\text{O})_n^+$ cluster which does not exhibit a depletion (but only a gain) signal in the HOH bending mode region.

The minimum energy isomer denoted as 3-a has a rhombic Mn_2O_2^+ cluster core with one intact water molecule bound to one of the Mn atoms as well as two water molecules which are deprotonated *via* hydroxylation of the cluster μ -oxo bridges. The binding of an intact water molecule yields a water bending vibration at 1577.5 cm^{-1} which should be clearly visible in the experimental IR-MPD spectrum. The first higher energy isomer 3-b (+0.29 eV higher in energy) is characterized by a bent Mn–OH–Mn unit which is bridged by an H_3O_2 unit yielding a distorted ring-like geometry. The H_3O_2 unit is formed by a hydroxylated cluster oxygen atom and an intact water molecule, *i.e.* the rhombic cluster core of isomer 3-a is opened upon dissociative water adsorption followed by an insertion of the adsorbed water. One more OH group is attached to each of the Mn atoms.

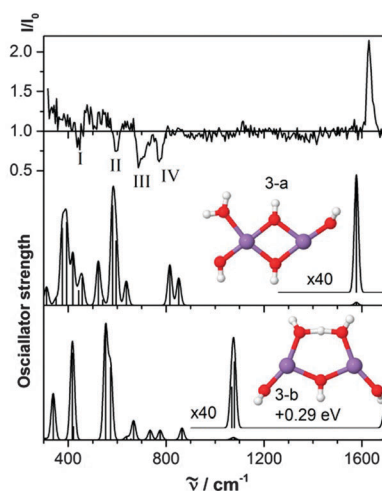


Fig. 5 IR-MPD spectrum (top panel) and calculated vibrational spectra of the two lowest energy isomeric structures of $\text{Mn}_2\text{O}_2(\text{H}_2\text{O})_3^+$; the ground-state (marked as 3-a) and the first higher-in-energy isomer (3-b). The calculated spectra (sticks) are convoluted with a Gaussian line shape function with a FWHM of 20 cm^{-1} . In the structural models, Mn, O, and H atoms are depicted as purple, red, and white spheres, respectively.

The formation of the H_3O_2 unit hinders the bending motion and thus considerably affects the vibrational frequency of the water bending mode which blue shifts to 1693.7 cm^{-1} . This value is at the edge of the wavenumber range of $300\text{--}1700\text{ cm}^{-1}$ experimentally studied and might thus not be detectable in the IR-MPD spectrum. Consequently, the absence of the HOH bending mode in the experimental IR-MPD spectrum of $\text{Mn}_2\text{O}_2(\text{H}_2\text{O})_3^+$ can be explained by the formation of an H_3O_2 unit and the associated shift of this mode to the edge of the detection range. A similar argument may also be invoked to explain the absence of water bending vibrations for $\text{Mn}_3\text{O}_3(\text{H}_2\text{O})_4^+$.

Next, we attempt to identify further characteristics in the vibrational spectra that may lend support to the presence of the theoretically predicted higher energy isomer 3-b in the measured spectra. The IR-MPD spectrum of $\text{Mn}_2\text{O}_2(\text{H}_2\text{O})_3^+$ exhibits four distinct signals at center wavenumbers of 441 cm^{-1} (labeled I), 597 cm^{-1} (II), 703 cm^{-1} (III), and 774 cm^{-1} (IV). The calculated vibrational spectrum of isomer 3-a shows numerous features below 700 cm^{-1} and two bands at 814.9 cm^{-1} and 851.3 cm^{-1} . None of these features can be clearly assigned to any of the experimentally observed signals. On the other hand, the calculated vibrational spectrum of isomer 3-b shows four clearly separated bands below 700 cm^{-1} as well as three more bands at 734.6 cm^{-1} , 775.4 cm^{-1} , and 864.6 cm^{-1} . This spectrum is in much more favorable agreement with the IR-MPD spectrum, in particular, the well separated measured signals I and II are nicely mirrored in the calculated spectrum and also the observed signals labeled III and IV are found in the calculated spectrum. In contrast, the feature at 864.6 cm^{-1} and the less intense predicted features at 1068.7 cm^{-1} and 1078.7 cm^{-1} are not observed in the experiment. Furthermore, the relative intensities of these modes in the measured and calculated spectra are different. This can be explained by two effects: (1) the laser intensity is not constant in the investigated spectral region which distorts the relative intensities of the signals. (2) Fragmentation of the complexes typically requires the absorption of multiple IR photons, where the absorbed energy is statistically re-distributed over the available vibrational degrees of freedom through intramolecular vibrational redistribution. The need for absorbing multiple photons makes the technique non-linear, and the observed IR intensities can generally deviate from the linear IR absorption, as theoretically predicted by calculations.²²

To ascertain whether the formation of H_3O_2 represents a general structural motif, we have studied theoretically the geometry of the entire series of $\text{Mn}_2\text{O}_2(\text{H}_2\text{O})_n^+$ ($n = 0\text{--}8$) complexes. Fig. 6 displays the calculated binding energies of up to eight water molecules to Mn_2O_2^+ . Shown are the binding energies as well as the structures for up to two isomers. Spatial spin distributions for the ground states and higher-energy spin-isomers for selected clusters displayed in Fig. 6 are shown in the ESI†; in particular we show spin isomers corresponding to $\text{Mn}_2\text{O}_2(\text{H}_2\text{O})_n^+$ ($n = 0, 4$ and 5) with the bare cluster corresponding to the one shown in the upper left corner of Fig. 6 and the other ones marked as 4-a and 5-a. As in the larger clusters shown in Fig. 4, we find that the lower energy states are characterized by maximal $\mu = N_\uparrow - N_\downarrow = 9$, regardless of the presence of water molecules.

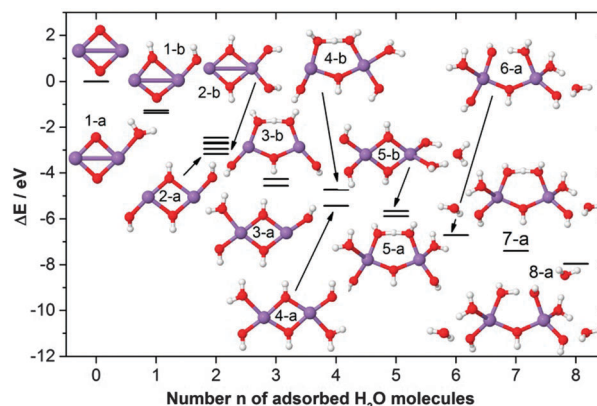


Fig. 6 Calculated binding energies of n water molecules to Mn_2O_2^+ for different isomeric structures (denoted as energy difference ΔE with respect to the bare rhombic Mn_2O_2^+ cluster, shown at the top left corner), plotted along with the corresponding structures. Mn, O, and H atoms are depicted as purple, red, and white spheres, respectively.

We further find the optimized geometry of the clusters is maintained for states with smaller μ , and that the spatial spin distributions (ferromagnetic for the maximal μ , and antiferromagnetic for smaller values of μ) show strong localization at Mn ion sites.

The bare Mn_2O_2^+ cluster is two-dimensional with a rhombic geometry.⁸ Adsorption of one intact water molecule does not change the geometry of the cluster core while the dissociative adsorption of H_2O ($+0.11\text{ eV}$ higher in energy) leads to a distortion of the rhombus. The minimum energy structures of all larger $\text{Mn}_2\text{O}_2(\text{H}_2\text{O})_n^+$ ($n > 1$) complexes contain two deprotonated water molecules and two hydroxylated cluster oxo-bridges. The first higher energy isomer of $\text{Mn}_2\text{O}_2(\text{H}_2\text{O})_2^+$ (denoted as 2-b) is comprised of two hydroxylated oxo-bridges as well as two OH groups bound to the same Mn atom. As aforementioned, the first higher energy isomer of $\text{Mn}_2\text{O}_2(\text{H}_2\text{O})_3^+$ shows that the diamond-shaped cluster structure can open and form a ring-like structure with an H_3O_2 unit. The same structural motif is also found for the first energy isomer of $\text{Mn}_2\text{O}_2(\text{H}_2\text{O})_4^+$. Most interesting is the finding that starting from $\text{Mn}_2\text{O}_2(\text{H}_2\text{O})_5^+$ this geometric structure becomes the lowest energy isomer. Two more water molecules are bound intact to the Mn atoms of the cluster while all further water molecules are attached *via* hydrogen bonds.

Additionally, the preferred formation of H_3O_2 units after adsorption of at least two water molecules has also been observed for the tetra-manganese tetra-oxide complexes $\text{Mn}_4\text{O}_4(\text{H}_2\text{O})_n^+$ (*cf.* Fig. 4).¹² Thus, the formation of an H_3O_2 unit appears to be cluster size independent and can thus be regarded as a general structural motif which is formed upon interaction of multiple water molecules with manganese oxide clusters.

In summary, the IR-MPD spectra in the characteristic HOH bending mode region together with a detailed theoretical analysis of the $\text{Mn}_2\text{O}_2(\text{H}_2\text{O})_n^+$ and $\text{Mn}_4\text{O}_4(\text{H}_2\text{O})_n^+$ complexes have shown that the interaction of water with manganese oxide clusters results in the deprotonation of water *via* hydroxylation of the cluster oxo-bridges. This mechanism already occurs for the first adsorbed water molecule and proceeds until all cluster O atoms

are hydroxylated, *i.e.* the number of water molecules which can be deprotonated is limited by the number of cluster oxygen atoms. However, for some clusters a depletion signal is observed for complexes containing less or the same number of water molecules as oxygen atoms ($n_{\max} < x + y$) which might arise from the stabilization of higher energy isomers. There is no obvious cluster size (number of Mn atoms in the cluster) or composition (number of oxygen atoms for a given number of Mn atoms) and thus formal Mn oxidation state dependence for the onset of the HOH bending mode. Furthermore, it has been shown for both Mn_2O_2^+ and Mn_4O_4^+ that the manganese oxide clusters are highly structurally fluxional and that adsorption of water can induce structural transformations of the cluster core.

3.4 Water induced oxygen dissociation

Besides the stoichiometric $\text{Mn}_x\text{O}_x(\text{H}_2\text{O})_n^+$ complexes we have also studied cluster complexes with one and two oxygen atoms in excess, respectively. To gain insight into the binding of the additional oxygen atoms it is instructive to explore the IR-MPD spectra at wavenumbers smaller than 1500 cm^{-1} .

According to Fig. 1, it is possible to divide the vibrational spectra in the range between 300 cm^{-1} and 1500 cm^{-1} into two characteristic regions. Independent of the cluster size, composition, and exact geometry of the $\text{Mn}_x\text{O}_{x+y}(\text{H}_2\text{O})_n^+$ complexes, there is typically a high density of states at wavenumbers smaller than 600 cm^{-1} which mainly arises from motions of the cluster core atoms. Recently,¹² we have shown for $\text{Mn}_4\text{O}_4(\text{H}_2\text{O})_{3-7}^+$ that this typically leads to a broad depletion band below 600 cm^{-1} . Due to the broad and unstructured nature of this band it does not serve as a good diagnostic for structural assignments or the basis for firm conclusions pertaining to the geometry of the $\text{Mn}_x\text{O}_{x+y}(\text{H}_2\text{O})_n^+$ complexes. In marked contrast, the spectral region between 600 cm^{-1} and 1500 cm^{-1} usually exhibits more distinct and better resolved signals which are more characteristic and thus more suitable for structural analysis.

As an example, Fig. 7a displays the IR-MPD spectrum of the cluster complex $\text{Mn}_2\text{O}_4(\text{H}_2\text{O})^+$ with two oxygen atoms in excess. In this case, no bands are visible for wavenumbers smaller than 600 cm^{-1} (labeled I). The lack of any signal in this spectral region is most likely caused by fragmentation of larger cluster complexes into $\text{Mn}_2\text{O}_4(\text{H}_2\text{O})^+$ in this frequency range, leading to an intensity gain for the mass of $\text{Mn}_2\text{O}_4(\text{H}_2\text{O})^+$ which results in obscuring the signal originating from vibrational motions characteristic to that species itself. In contrast, an intense signal in the region between 630 cm^{-1} and 730 cm^{-1} (labeled II) and two less intense signals around $785\text{--}810\text{ cm}^{-1}$ (labeled III) are visible, which arise mainly from librations and rotations of OH groups. Furthermore, two additional signals with band centers at 1148 cm^{-1} and 1125 cm^{-1} (labeled IV) are detected.

Successively increasing the number of adsorbed water molecules (Fig. 7b–e) leads to a continuous change of the IR-MPD spectra. First, we observe the expected appearance of a broad, unstructured band below 600 cm^{-1} (labeled I). Secondly, the band between 630 cm^{-1} and 730 cm^{-1} (II) appears to broaden while the signals labeled III disappear. However, the most interesting development is that of the evolution of band IV: the double

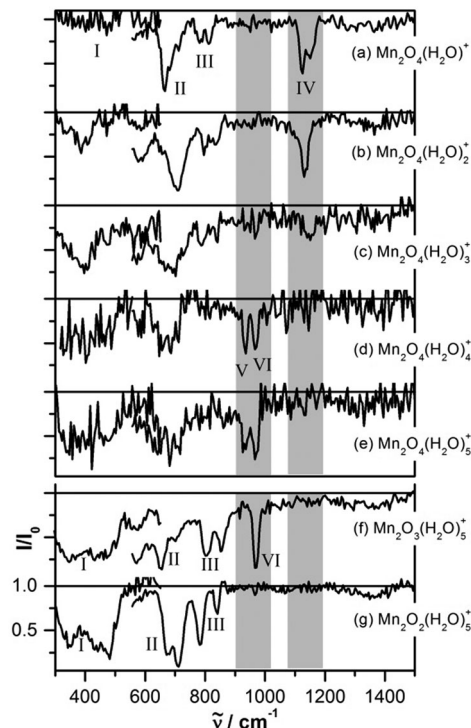


Fig. 7 IR-MPD spectra of (a–e) the cluster complexes $\text{Mn}_2\text{O}_4(\text{H}_2\text{O})_n^+$ ($n = 1\text{--}5$) with two oxygen atoms in excess, (f) the cluster complex $\text{Mn}_2\text{O}_3(\text{H}_2\text{O})_5^+$ with one oxygen atom in excess, as well as (g) the stoichiometric $\text{Mn}_2\text{O}_2(\text{H}_2\text{O})_5^+$ cluster, in the spectral region of $300\text{--}1500\text{ cm}^{-1}$. Plotted is the mass signal intensity ratio I/I_0 with (I) and without (I_0) laser light as a function of the laser wavenumber $\tilde{\nu}$.

band for $\text{Mn}_2\text{O}_4(\text{H}_2\text{O})^+$ becomes a single band with a band center at 1131 cm^{-1} for $\text{Mn}_2\text{O}_4(\text{H}_2\text{O})_2^+$. Upon addition of a third water molecule (*cf.* Fig. 7c) the intensity of this signal becomes very small and finally it disappears starting from $\text{Mn}_2\text{O}_4(\text{H}_2\text{O})_4^+$. Instead, two new signals with band centers at 934 cm^{-1} and 967 cm^{-1} (labeled V and VI) appear. These features are retained for all larger investigated complexes containing up to six water molecules (*cf.* Fig. 7e and 8a).

A rather similar IR-MPD spectrum is observed for the corresponding cluster complex $\text{Mn}_2\text{O}_3(\text{H}_2\text{O})_5^+$ with one oxygen atom in excess (Fig. 7f). Besides the broad unstructured band below 600 cm^{-1} (I) more distinct features are observed above 600 cm^{-1} . The broad band II of $\text{Mn}_2\text{O}_4(\text{H}_2\text{O})_{2-5}^+$ becomes better resolved and two signals between 780 cm^{-1} and 890 cm^{-1} appear which are similar to the signals marked III in the spectrum of $\text{Mn}_2\text{O}_4(\text{H}_2\text{O})^+$. In addition, similar to the band VI of $\text{Mn}_2\text{O}_4(\text{H}_2\text{O})_{4-6}^+$ a high intensity signal with a band center at 969 cm^{-1} is observed. Fig. 8 shows that this signal is observed for all investigated $\text{Mn}_2\text{O}_3(\text{H}_2\text{O})_n^+$ complexes containing between four and eight water molecules and thus it appears to be characteristic for the cluster complexes $\text{Mn}_2\text{O}_3(\text{H}_2\text{O})_n^+$ with one oxygen atom in excess.

A similar spectrum is also detected for the corresponding stoichiometric $\text{Mn}_2\text{O}_2(\text{H}_2\text{O})_5^+$ complex (Fig. 7g) in the spectral region between 300 cm^{-1} and 900 cm^{-1} . All features labeled I–III are visible, though the relative intensities of the signal are slightly different. Most importantly, however, the characteristic signal

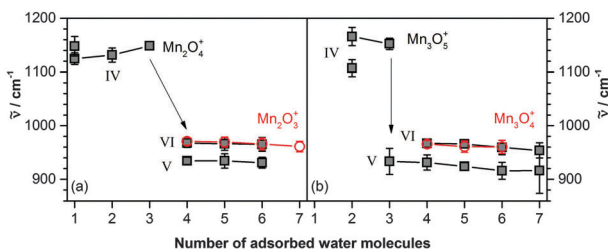


Fig. 8 Experimentally obtained band centers of signals observed in two characteristic spectral regions as a function of the number of adsorbed water molecules. (a) Signals for the di-manganese oxide clusters $\text{Mn}_2\text{O}_3(\text{H}_2\text{O})_n^+$ ($n = 4-7$) (shown as red open circles) and $\text{Mn}_2\text{O}_4(\text{H}_2\text{O})_n^+$ ($n = 1-6$) (black filled squares). (b) Signals for the tri-manganese oxide clusters $\text{Mn}_3\text{O}_4(\text{H}_2\text{O})_n^+$ ($n = 4-6$) (red open circles) and $\text{Mn}_3\text{O}_5(\text{H}_2\text{O})_n^+$ ($n = 2-7$) (black filled squares). The error bars represent the FWHM. The lines are drawn to guide the eye. The labels IV, V, and VI refer to the signals in Fig. 7.

at 969 cm^{-1} is not visible anymore in the spectrum of $\text{Mn}_2\text{O}_2(\text{H}_2\text{O})_5^+$ and is also not observed for any other investigated water complex of Mn_2O_2^+ .

This composition and water dependent behavior of the characteristic signals around $930-970\text{ cm}^{-1}$ and $1120-1150\text{ cm}^{-1}$ is not unique for the di-manganese oxide clusters but is also observed for the tri-manganese oxide series. Fig. 8b shows that the cluster complex $\text{Mn}_3\text{O}_5(\text{H}_2\text{O})_2^+$ with two oxygen atoms in excess manifests a double band with band centers at 1107 cm^{-1} and 1166 cm^{-1} which becomes a single band with a band center at 1152 cm^{-1} for $\text{Mn}_3\text{O}_5(\text{H}_2\text{O})_3^+$ (analog to IV of $\text{Mn}_2\text{O}_4(\text{H}_2\text{O})_{1-3}^+$ in Fig. 7a-c and 8a). The intensity of this band decreases with increasing water content and a new double peak feature with two bands around 925 cm^{-1} and 960 cm^{-1} appears (analog to V and VI for $\text{Mn}_2\text{O}_4(\text{H}_2\text{O})_{3-6}^+$ in Fig. 7d, e and 8a). In analogy with the signal marked VI for $\text{Mn}_2\text{O}_3(\text{H}_2\text{O})_{2-7}^+$ (cf. Fig. 7f and 8a), the complexes $\text{Mn}_3\text{O}_4(\text{H}_2\text{O})_{4-6}^+$ with one oxygen atom in excess also exhibit a feature around 960 cm^{-1} . Similar trends are also observed for the complexes $\text{Mn}_4\text{O}_5(\text{H}_2\text{O})_n^+$ (not shown here).

Now the questions arise, whether the features labeled IV, V, and VI can be assigned to any specific vibrational modes and why the latter two disappear with decreasing number of water molecules adsorbed on the clusters with two oxygen atoms in excess. Previous infrared spectroscopic investigations of MnO_2 in cold argon and nitrogen matrices revealed modes at 948.0 cm^{-1} , 962.4 cm^{-1} , and 969.6 cm^{-1} which have all been assigned to the asymmetric stretching vibration of a bent O-Mn-O unit.²³ A similar mode has also been observed for larger manganese oxide clusters. An early study of solid $\text{Mn}_2\text{O}_7(\text{H}_2\text{O})_2$ showed a signal at 943 cm^{-1} which has been assigned to the asymmetric stretch of an MnO_3 unit.²⁴ Later the same mode was observed for Mn_2O_7 in the absence of any matrix at 955 cm^{-1} , whereas it has been found to shift to $953-958\text{ cm}^{-1}$ and $949-960\text{ cm}^{-1}$ in the presence of a nitrogen and argon matrix, respectively.²⁵ Furthermore, the vibration of the diatomic MnO in a cold argon matrix²³ has been observed at around 833 cm^{-1} . Based on these assignments and the observation that the signals around $960-970\text{ cm}^{-1}$ are not present for any of the stoichiometric $\text{Mn}_x\text{O}_x(\text{H}_2\text{O})_n^+$ ($x = 2-5$) complexes but only

appear for the clusters $\text{Mn}_2\text{O}_3(\text{H}_2\text{O})_n^+$, $\text{Mn}_3\text{O}_4(\text{H}_2\text{O})_n^+$, and $\text{Mn}_4\text{O}_5(\text{H}_2\text{O})_n^+$ with one oxygen atom in excess as well as some of the cluster complexes with two oxygen atoms in excess, $\text{Mn}_2\text{O}_4(\text{H}_2\text{O})_n^+$ and $\text{Mn}_3\text{O}_5(\text{H}_2\text{O})_n^+$, it can be concluded that this feature most likely arises from the stretch motion of an oxygen atom terminally bound to one of the manganese atoms. This assignment is further confirmed by the appearance of a single signal (VI) for the complexes with one oxygen atom in excess and a double peak (V and VI) for the complexes with two oxygen atoms in excess. The complexes with one oxygen atom in excess contain only one terminal oxygen atom leading to a single peak in the IR-MPD spectra while the complexes with two oxygen atoms in excess can yield two differently bound terminal O atoms which is reflected in the double peak structure of the IR-MPD signal.

In contrast, we assign the signals labeled IV around $1120-1150\text{ cm}^{-1}$ to an O-O stretch mode of an intact O_2 molecule. This assignment is based on the observation that feature IV is only present for the complexes $\text{Mn}_2\text{O}_4(\text{H}_2\text{O})_n^+$ and $\text{Mn}_3\text{O}_5(\text{H}_2\text{O})_n^+$ with two oxygen atoms in excess whereas it is not detected for the cluster complexes with one oxygen atom in excess and stoichiometric complexes. Furthermore, corresponding gain signals are observed in the $\text{Mn}_2\text{O}_2(\text{H}_2\text{O})_n^+$ and $\text{Mn}_3\text{O}_3(\text{H}_2\text{O})_n^+$ mass channels which demonstrate the fragmentation of $\text{Mn}_2\text{O}_4(\text{H}_2\text{O})_n^+$ and $\text{Mn}_3\text{O}_5(\text{H}_2\text{O})_n^+$ via loss of an O_2 molecule. In addition, a previous study on cyclic and end-bonded manganese di-oxide MnO_2 in a cold nitrogen or argon matrix found the O-O stretch at about 1108 cm^{-1} and 1230 cm^{-1} , respectively.²³ Similarly, IR-MPD spectra of bare $\text{Mn}_x\text{O}_{x+y}^+$ ($x = 2-5$, $y = 0-2$) clusters with an additional intact O_2 molecule attached (serving as messenger) also showed a similar band between 1100 cm^{-1} and 1200 cm^{-1} , which has been assigned to the O-O stretch mode of the dioxygen species.²⁶ The disappearance of this signal with increasing number of adsorbed water molecules in conjunction with the appearance of the signals marked as V and VI in Fig. 7, is further evidence that the originally intact O_2 molecule dissociates upon adsorption of a critical number of water molecules. This process results in a cluster with terminally bound oxygen atoms as in the case of $\text{Mn}_x\text{O}_{x+1}^+$ with one oxygen atom in excess. For computational investigation of the bonding of a terminal oxygen atom in both the neutral and charged Mn_2O_3 molecule see the ESI.†

The observation of terminally bound oxygen species is particularly interesting pertaining to the ongoing discussion about the mechanism for O-O bond formation in the natural OEC. So far different mechanisms have been proposed which involve oxygen moieties that are terminally coordinated or bridged between two metal atoms. The most likely mechanism among these describes the O-O bond formation via interaction of a μ_3 -oxo-bridge and a terminal oxygen atom as recently deduced by the use of time-resolved membrane inlet mass spectrometry.²⁷ This experimentally determined mechanism is in agreement with theoretical predictions by Siegbahn.²⁸ However, the nature of this terminal oxygen species is not clear yet and the involvement of both, a Mn^{IV} -oxyl radical and the isoelectronic Mn^{V} -oxo center have been proposed. Based on the investigation of

synthetic Mn-oxo species, Borovik and coworkers suggested recently the consideration of a high spin Mn^V-oxo center instead of a Mn-oxyl radical for the O–O bond.²⁹

4. Conclusions

In this contribution we report on a comprehensive experimental and theoretical investigation of the deprotonation of water on free manganese oxide clusters. Using infrared multiple-photon dissociation spectroscopy in conjunction with first-principles spin density functional theory calculations of several series of water complexes Mn_xO_{x+y}(H₂O)_n⁺ comprising between two and five Mn atoms, allows for the identification of general trends and concepts which describe the interaction of water with manganese oxide clusters. These include:

(1) The interaction of water with manganese oxide clusters leads to facile deprotonation of the water molecules *via* hydroxylation of cluster oxo-bridges independent of the cluster size and the cluster composition.

(2) Water deprotonation already occurs for the first H₂O molecule interacting with the cluster and cooperative effects of multiple adsorbed water molecules are not necessary for this process.

(3) Due to the deprotonation *via* oxo-bridge hydroxylation, the number of deprotonated water molecules is limited by the number of available cluster oxo-bridges.

(4) Further water molecules are bound molecularly (intact) and the formation of hydrogen-bridge-bound H₃O₂ units involving the hydroxylated oxo-bridges is the preferred structural motif.

(5) The formal oxidation state of the Mn atoms was not found to have any obvious influence on the deprotonation of the water molecules, while, previous studies^{4,13} demonstrated the importance of the formal Mn oxidation state for water oxidation.

(6) The manganese oxide clusters are highly structurally fluxional and water adsorption can induce considerable structural transformations of the manganese oxide cluster core, including dimensional crossover from 2D to 3D structures.

(7) Clusters Mn_xO_{x+1}⁺ with one oxygen atom in excess contain a terminal O atom.

(8) In contrast, clusters Mn_xO_{x+2}⁺ with two oxygen atoms in excess contain an intact O₂ unit which, however, dissociates upon adsorption of a critical number of water molecules to form two terminal O atoms.

Acknowledgements

We gratefully acknowledge the Stichting voor Fundamenteel Onderzoek der Materie (FOM) for the support of the FELIX Laboratory. The research leading to these results has received funding from the European Community's Seventh Framework Programme (FP7/2007–2013) under grant agreement no. 312284. S. M. L. is grateful to the ESF Baden-Württemberg for a Margarete von Wrangell fellowship. R. N. B. was supported by grant no. FG05-86ER45234 from the Office of Basic Energy Sciences of the US Department of energy (DOE) and U. L. by the Air Force Office

for Scientific Research (AFOSR). Computations were carried out at the Georgia Tech Center for Computational Materials Science. D. K. acknowledges support from the Netherlands Organisation for Scientific Research (NWO) as part of the Dutch Astrochemistry Network.

Notes and references

- M. Suga, F. Akita, K. Hirata, G. Ueno, H. Murakami, Y. Nakajima, T. Shimizu, K. Yamashita, M. Yamamoto, H. Ago and J.-R. Shen, *Nature*, 2015, **517**, 99; Y. Umena, K. Kawakami, J.-R. Shen and N. Kamiya, *Nature*, 2011, **473**, 55.
- J.-R. Shen, *Annu. Rev. Plant Biol.*, 2015, **66**, 23.
- J. Yano and V. Yachandra, *Chem. Rev.*, 2014, **114**, 4175–4205; J. P. McEvoy and G. W. Brudvig, *Chem. Rev.*, 2006, **106**, 4455; H. Dau, I. Zaharieva and M. Haumann, *Curr. Opin. Chem. Biol.*, 2012, **16**, 3.
- H. Dau, C. Limberg, T. Reier, M. Risch, S. Roggan and P. Strasser, *ChemCatChem*, 2010, **2**, 724.
- M. Yagi and M. Kaneko, *Chem. Rev.*, 2001, **101**, 21; S. Mukhopadhyay, S. K. Mandal, S. Bhaduri and W. H. Armstrong, *Chem. Rev.*, 2004, **104**, 3981; R. Brimblecombe, G. F. Swiegers, G. C. Dismukes and L. Spiccia, *Angew. Chem., Int. Ed.*, 2008, **47**, 7335; G. C. Dismukes, R. Brimblecombe, G. A. N. Felton, R. S. Pryadun, J. E. Sheats, L. Spiccia and G. F. Swiegers, *Acc. Chem. Res.*, 2009, **42**, 1935; J. S. Kanady, E. Y. Tsui, M. W. Day and T. Agapie, *Science*, 2011, **333**, 733; J. S. Kanady, P.-H. Lin, K. L. Carsch, R. J. Nielsen, M. K. Takase, W. A. Goddard III and T. Agapie, *J. Am. Chem. Soc.*, 2014, **136**, 14373; C. Zhang, C. Chen, H. Dong, J.-R. Shen, H. Dau and J. Zhao, *Science*, 2015, **348**, 690.
- M. Wiechen, H.-M. Berends and P. Kurz, *Dalton Trans.*, 2012, **41**, 41.
- M. M. Najafpour, T. Ehrenberg, M. Wiechen and P. Kurz, *Angew. Chem., Int. Ed.*, 2010, **49**, 2233; N. Birkner, S. Nayeri, B. Pashaei, M. M. Najafpour, W. H. Casey and A. Navrotsky, *Proc. Natl. Acad. Sci. U. S. A.*, 2013, **110**, 8801; M. Wiechen, M. M. Najafpour, S. I. Allakhverdiev and L. Spiccia, *Energy Environ. Sci.*, 2014, **7**, 2203.
- S. M. Lang, I. Fleischer, T. M. Bernhardt, R. N. Barnett and U. Landman, *Nano Lett.*, 2013, **13**, 5549.
- S. M. Lang, I. Fleischer, T. M. Bernhardt and R. N. Barnett, *J. Phys. Chem. C*, 2015, **119**, 10881.
- S. K. Nayak and P. Jena, *Phys. Rev. Lett.*, 1998, **81**, 2970; S. K. Nayak and P. Jena, *J. Am. Chem. Soc.*, 1999, **121**, 644.
- S. Datta and B. Rahaman, *AIP Adv.*, 2015, **5**, 117231.
- S. M. Lang, T. M. Bernhardt, D. M. Kiawi, J. M. Bakker, R. N. Barnett and U. Landman, *Angew. Chem., Int. Ed.*, 2015, **127**, 15328.
- H. Dau and M. Haumann, *Coord. Chem. Rev.*, 2008, **252**, 273; V. Krewald, F. Neese and D. A. Pantazis, *Isr. J. Chem.*, 2015, **55**, 1219; V. Krewald, M. Retegan, N. Cox, J. Messinger, W. Lubitz, S. DeBeer, F. Neese and D. A. Pantazis, *Chem. Sci.*, 2015, **6**, 1676.

- 14 D. Oepts, A. F. G. van der Meer and P. W. van Amersfoort, *Infrared Phys. Technol.*, 1995, **36**, 297; A. Fielicke, G. von Helden, G. Meijer, B. Simard, S. Dénomée and D. M. Rayner, *J. Am. Chem. Soc.*, 2003, **125**, 11184.
- 15 R. N. Barnett and U. Landman, *Phys. Rev. B: Condens. Matter Mater. Phys.*, 1993, **48**, 2081.
- 16 N. Troullier and J. L. Martins, *Phys. Rev. B: Condens. Matter Mater. Phys.*, 1991, **43**, 1993.
- 17 J. P. Perdew, K. Burke and M. Ernzerhof, *Phys. Rev. Lett.*, 1996, **77**, 3865.
- 18 D. Porezag and M. R. Pederson, *Phys. Rev. B: Condens. Matter Mater. Phys.*, 1996, **54**, 7830.
- 19 P. Giazzoni and S. Baroni, *J. Chem. Phys.*, 1994, **100**, 8537.
- 20 R. A. Toth, *J. Mol. Spectrosc.*, 1998, **190**, 379; T. Shimanouchi, *Tables of Molecular Vibrational Frequencies Consolidated*, National Bureau of Standards, 1972, vol. 1.
- 21 C. Kerpel, D. J. Harding, D. M. Rayner and A. Fielicke, *J. Phys. Chem. A*, 2013, **117**, 8230; A. Fielicke, R. Mitrić, G. Meijer, V. Bonačić-Koutecký and G. von Helden, *J. Am. Chem. Soc.*, 2003, **125**, 15716.
- 22 J. Oomens, B. G. Sartakov, G. Meijer and G. von Helden, *Int. J. Mass Spectrom.*, 2006, **254**, 1.
- 23 G. V. Chertihin and L. Andrews, *J. Phys. Chem. A*, 1997, **101**, 8547.
- 24 B. Krebs and K.-D. Hasse, *Z. Naturforsch.*, 1973, **28b**, 218.
- 25 W. Levason, J. S. Ogden and J. W. Turff, *J. Chem. Soc., Dalton Trans.*, 1983, 2699.
- 26 C. van Dijk, *Structure and Magnetism of Atomic Clusters*, PhD thesis, Radboud University Nijmegen, The Netherlands, 2011.
- 27 N. Cox and J. Messinger, *Biochim. Biophys. Acta*, 2013, **1827**, 1020; W. Hillier and T. Wydrzynski, *Biochemistry*, 2000, **39**, 4399.
- 28 P. E. M. Siegbahn, *J. Am. Chem. Soc.*, 2013, **135**, 9442.
- 29 R. Gupta, T. Taguchi, B. Lassalle-Kaiser, E. L. Bominaar, J. Yano, M. P. Hendrich and A. S. Borovik, *Proc. Natl. Acad. Sci. U. S. A.*, 2015, **112**, 5319.